Int. J. Heat Mass Transfer. Vol. 33, No. 7, pp. 1465–1474, 1990
Printed in Great Britain

0017-9310/90 $3.00 + 0.00
Pergamon Press plc

# Condensation of a vapour with incondensables: an improved gas phase film model accounting for the effect of mass transfer on film thickness

A. C. BANNWART† and A. BONTEMPS‡

Groupement pour la Recherche sur les Echangeurs Thermiques, Service des Transferts Thermiques, Laboratoire d'Etudes Thermiques des Echangeurs, Commissariat à l'Energie Atomique, Centre d'Etudes Nucleaires de Grenoble, 85X-38041 Grenoble Cedex, France

(*Received* 28 *April* 1989 *and in final form* 14 *August* 1989)

**Abstract**—An improved gas phase film model is presented for calculation of local skin friction, heat and mass transfer coefficients in condenser design. The model accounts for the effect of the local mass transfer intensity on film thickness in turbulent flow. Predictions from the proposed model and from the classical 'film theory' and 'condensation curve' methods are compared with experimental data for a saturated steam–air mixture inside a 2 cm diameter tube under the following conditions: pressure, 1–1.5 bar; air mass fraction, 2–30%; inlet velocity, 5–50 m $s^{-1}$. Results indicate that for low values of the heat flux density (and for low values of the condensation rate) the three methods above are in excellent agreement with data. For high values of the heat flux density, the proposed model gives excellent agreement with the data but the classical methods do not.

## 1. INTRODUCTION

DETERMINATION OF local transfer coefficients during condensation in the presence of noncondensables is a major task in designing condensers. Two types of standard design theory are currently in use [1–3]: (a) 'film theory' models [4–7], based on a simplified analysis of the momentum, heat and mass transfer gas phase equations near the condensate interface; and (b) 'condensation curve' methods [8, 9], based on the calculation of an equilibrium temperature/specific enthalpy curve for the two-phase mixture, thus ignoring phenomena (mainly mass diffusion) associated with the real nonequilibrium between phases.

A formal comparison between these two methods [1] shows that they give the same local results only when the gas Lewis number is unity and the mass transfer driving force is small. Otherwise the film theory model is preferred.

Derivation of the film theory is presented at a fundamental level by Bird *et al.* [10], and reviewed in detail by one of the authors [11].

The crucial point of the analysis is the closure conditions assuming that the equivalent thickness of the laminar film is invariant under mass transfer, allowing one to eliminate it in the rest of the derivation. This is in contradiction with the well-known fact that in a turbulent flow the viscous sublayer thickness is an increasing function of the suction rate at the wall [12–17]. Since this thickness directly 'controls' the slope of the velocity profile, it must affect the heat and mass transfer coefficients as well.

The main objective of this paper is to develop an analytical film model accounting for the effect above. This is done by introducing a very simple turbulence model which is valid in the near-interface region (viscous sublayer). The final correlations obtained for the transfer coefficients are easily compared with those furnished by classical film theory and condensation curve methods. In order to check the proposed model, measurements of mean heat flux have been taken for condensation of steam in the presence of air inside a tube (Section 3).

## 2. ANALYTICAL MODEL

The conservation equations for the gas phase in a thin layer near a smooth interface are discussed by Bird *et al.* [10]. For turbulent flow condensation of a vapour in the presence of a gas, we can write them as (Fig. 1):

mass transfer

$$m_{v,i}(1-Y_{v,i}) = m_{v,i}(Y_v - Y_{v,i}) + c\mathcal{M}_v(\mathcal{D}+\varepsilon_D)\frac{dY_v}{dy}; \quad (1)$$

heat transfer

$$\varphi_i = m_{v,i}c_{p,v}(T-T_i) + \rho c_p(\alpha+\varepsilon_T)\frac{dT}{dy}; \quad (2)$$

† Present address: Universidade Estadual de Campinas, FEC, Departament de Energia, 13081 Campinas, SP, Brazil.

‡ Present address: Université Joseph Fourier, Grenoble, France.

## NOMENCLATURE

| | |
|---|---|
| $b$ | parameter |
| $c$ | molar density of the mixture [kmol m$^{-3}$] |
| $c_p$ | specific heat capacity at constant pressure [J kg$^{-1}$ K$^{-1}$] |
| $c_{p,g}$ | specific heat capacity at constant pressure of the noncondensable gas [J kg$^{-1}$ K$^{-1}$] |
| $c_{p,v}$ | specific heat capacity at constant pressure of the condensable vapour [J kg$^{-1}$ K$^{-1}$] |
| $C_f$ | skin friction coefficient |
| $\mathscr{D}$ | diffusivity [m$^2$ s$^{-1}$] |
| $h$ | heat transfer coefficient [W m$^{-2}$ K$^{-1}$] |
| $h_D$ | mass transfer coefficient [m s$^{-1}$] |
| $I(\xi)$ | integral defined in equation (19) |
| $K$ | Von Karman constant, 0.41 |
| $\mathscr{L}$ | latent heat of vaporization [J kg$^{-1}$] |
| $M_g$ | mass flow rate of noncondensable gas [kg s$^{-1}$] |
| $M_v$ | mass flow rate of vapour [kg s$^{-1}$] |
| $m_{v,i}$ | mass transfer flux at interface [kg m$^{-2}$ s$^{-1}$] |
| $\mathscr{M}_v$ | molar mass of vapour [kg kmol$^{-1}$] |
| $P$ | pressure [N m$^{-2}$] |
| $Pr$ | Prandtl number |
| $Pr_t$ | turbulent Prandtl number |
| $P_v$ | partial pressure of vapour [N m$^{-2}$] |
| $Q$ | average heat transfer rate [W] |
| $R_D$ | mass transfer driving force, $(Y_{v,m}-Y_{v,i})/(1-Y_{v,i})$ |
| $Sc$ | Schmidt number |
| $Sc_t$ | turbulent Schmidt number |
| $St$ | heat transfer Stanton number |
| $T$ | temperature [K] |
| $u$ | velocity [m s$^{-1}$] |
| $y$ | coordinate normal to the interface [m] |
| $y_s$ | nominal viscous sublayer thickness [m] |
| $Y_v$ | molar fraction of vapour. |

Greek symbols

| | |
|---|---|
| $\alpha$ | thermal diffusivity [m$^2$ s$^{-1}$] |
| $\beta$ | parameter |
| $\gamma$ | $y_{s,0}/y_s$ |
| $\varepsilon$ | hydrodynamic turbulent diffusivity [m$^2$ s$^{-1}$] |
| $\eta$ | $y/y_s$ |
| $\lambda$ | thermal conductivity [W m$^{-1}$ K$^{-1}$] |
| $\mu$ | dynamic viscosity [kg m$^{-1}$ s$^{-1}$] |
| $\nu$ | kinematic viscosity [m$^2$ s$^{-1}$] |
| $\rho$ | density [kg m$^{-3}$] |
| $\tau_i$ | shear stress at interface [N m$^{-3}$] |
| $\varphi_i$ | heat flux at interface [W m$^{-2}$] |
| $\Phi$ | $2m_{v,i}/u_m C_{f,0}\rho$ |
| $\Phi_T$ | $m_{v,i}c_{p,v}/h_0$ |
| $\Psi$ | parameter. |

Subscripts

| | |
|---|---|
| D | diffusional |
| f | friction |
| g | noncondensable gas |
| i | at the interface |
| in | at the inlet of the test section |
| m | bulk value |
| out | at the outlet of the test section |
| s | at the viscous sublayer boundary |
| sat | at saturation conditions |
| t | turbulent |
| T | thermal |
| v | vapour |
| 0 | in the absence of mass transfer. |

Superscripts

| | |
|---|---|
| + | dimensionless with respect to $\tau_i$, $\rho$, $\nu$ |
| * | at equilibrium between phases. |

skin friction

$$\tau_i = m_{v,i}(u-u_i)+\rho(\nu+\varepsilon)\frac{du}{dy} \tag{3}$$

where $m_{v,i}$ is the vapour mass flux at the liquid–gas interface ($y=0$) and $Y_v$ is the molar fraction of the vapour. The terms $\varepsilon_D$, $\varepsilon_T$ and $\varepsilon$ are respectively the eddy mass diffusivity, the eddy thermal diffusivity and the eddy viscosity. Other terms have the usual notation.

In these equations, the transfer coefficients are defined to be proportional to the diffusion fluxes at the liquid–vapour interface

$$h_D = \frac{m_{v,i}(1-Y_{v,i})}{c\mathscr{M}_v(Y_{v,m}-Y_{v,i})} = \frac{m_{v,i}}{c\mathscr{M}_v R_D} \tag{4}$$

$$h = \frac{\varphi_i}{T_m - T_i} \tag{5}$$

$$C_f = \frac{\tau_i}{\frac{1}{2}\rho(u_m-u_i)^2} \tag{6}$$

where $R_D = (Y_{v,m}-Y_{v,i})/(1-Y_{v,i})$ is the normalized difference of the vapour molar fractions representing the mass transfer driving force.

In the vicinity of the interface, it can be proved from continuity considerations [12] that

$$\varepsilon = O(y^3) \quad \text{for } y \to 0. \tag{7}$$

This is the so-called Reichardt criterion, which is valid in the viscous sublayer. Scaling equation (7), we have

$$\frac{\varepsilon}{\nu} = \left(\frac{\varepsilon}{\nu}\right)_s\left(\frac{y}{y_s}\right)^3. \tag{8}$$

In order to obtain the scales in the above equation, we adopt temporarily a 'two-layer' picture for the

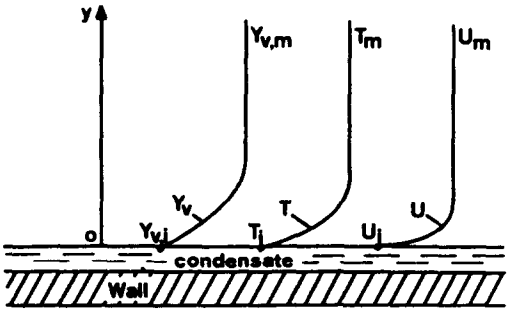


FIG. 1. Schematic diagram of the velocity ($u$), temperature ($T$) and vapour fraction ($Y_v$) profiles near the liquid–gas interface as a function of the $y$-coordinate (perpendicular to the fluid motion). The subscripts m and i refer to the bulk and interface values, respectively.

velocity profile. Let us assume that at the boundary $y = y_s$ for the viscous sublayer, and $\varepsilon/\nu$ satisfies Prandtl's generalized mixing length theory [17]

$$\frac{1}{K}\left(\frac{\varepsilon}{\nu}\right)_s = \frac{y_s\sqrt{(\tau_s/\rho)}}{\nu} = y_s^+\sqrt{\left(\frac{\tau_s}{\tau_i}\right)}. \tag{9}$$

Since this parameter has the character of a local transition Reynolds number, we assume after Kendall *et al.* [12] that it has the *same* value when the viscous sublayer velocity profile intercepts the fully turbulent profile (at $y_s$), whatever the mass transfer flux. This value can thus be obtained from velocity profile data in the absence of mass transfer. In this case, the viscous sublayer linear profile meets the logarithmic profile when

$$\frac{1}{K}\left(\frac{\varepsilon}{\nu}\right)_s = y_{s,0}^+ \cong 10.7 \tag{10}$$

from Clauser's data [18]. Equations (9) and (10) give $y_s^+$ as a function of $\tau_s$.

The latter is obtained by integrating equation (3) far from the liquid–vapour interface where $\nu \ll \varepsilon$. After Kendall *et al.* [12], the velocity profile can be written as

$$u-u_i = \frac{\tau_i}{m_{v,i}}\left\{1-\left[\frac{m_{v,i}}{2K\sqrt{(\rho\tau_i)}}\ln\left(\frac{y}{y_s}\right) - \exp\left(-\frac{m_{v,i}y_s}{2\mu}\right)\right]^2\right\}. \tag{11}$$

For $y = y_s$, we obtain $\tau_s$ as

$$\tau_s = \tau_i - m_{v,i}(u_s-u_i) = \tau_i\exp\left(-\frac{m_{v,i}y_s}{\mu}\right). \tag{12}$$

This completes the determination of the scales in equation (7). Thus, the turbulence model near the interface (viscous sublayer) is

$$\frac{\varepsilon}{\nu} = Ky_{s,0}^+\left(\frac{y}{y_s}\right)^3 \tag{13}$$

where, from equations (9), (10) and (12)

$$y_s^+ = y_{s,0}^+\exp\left(\tfrac{1}{2}\cdot\frac{m_{v,i}y_s}{\mu}\right) \tag{14}$$

with $y_{s,0}^+$ given by equation (10). Taking as usual [13, 17]

$$Pr_t = \frac{\varepsilon}{\varepsilon_T} = \text{const.}$$

$$Sc_t = \frac{\varepsilon}{\varepsilon_D} = \text{const.} \tag{15}$$

and taking into account the turbulence model given by equation (13), equations (1)–(3) become

$$m_{v,i}(1-Y_{v,i}) = m_{v,i}(Y_v - Y_{v,i}) + c\mathcal{M}_v\mathcal{D}\left[1+\frac{Sc}{Sc_t}Ky_{s,0}^+\left(\frac{y}{y_s}\right)^3\right]\frac{dY_v}{dy} \tag{16}$$

$$\varphi_i = m_{v,i}c_{p,v}(T-T_i) + \rho c_p\alpha\left[1+\frac{Pr}{Pr_t}Ky_{s,0}^+\left(\frac{y}{y_s}\right)^3\right]\frac{dT}{dy} \tag{17}$$

$$\tau_i = m_{v,i}(u-u_i) + \rho\nu\left[1+Ky_{s,0}^+\left(\frac{y}{y_s}\right)^3\right]\frac{du}{dy}. \tag{18}$$

Integration of the above equations yields the profiles near the interface as functions of integrals of the following form:

$$I(b\eta) = \int_0^\eta \frac{b\,d\eta}{1+(b\eta)^3} \tag{19}$$

where

$$\eta = \frac{y}{y_s} \tag{20a}$$

$$b = \left(\frac{Sc}{Sc_t}Ky_{s,0}^+\right)^{1/3}, \quad \left(\frac{Pr}{Pr_t}Ky_{s,0}^+\right)^{1/3}, \quad (Ky_{s,0}^+)^{1/3}. \tag{20b}$$

Since we are concerned with correlating the transfer coefficients in a simple way, we impose the bulk conditions in the profiles as

$$Y_v(\infty) = Y_{v,m}$$
$$T(\infty) = T_m$$
$$u(\infty) = u_m \tag{21}$$

and the above integrals become

$$I(b\eta) = I(\infty) = \frac{2\pi}{3\sqrt{3}}.$$

With the above conditions, the profiles are solved for $m_{v,i}$, $\varphi_i$ and $\tau_i$ resulting in the following expressions for the transfer coefficients:

$$h_D = \frac{1}{I(\infty)}\left(\frac{Ky^+_{s,0}}{Sc_t}\right)^{1/3}\left(\frac{\mathscr{D}\,Sc^{1/3}}{y_s}\right)\frac{\ln(1-R_D)^{-1}}{R_D} \quad (22)$$

$$h = \frac{m_{v,i}c_{p,v}}{1-\exp\left[-I(\infty)\left(\frac{Pr_t}{Ky^+_{s,0}}\right)^{1/3}\left(\frac{y_s}{\lambda\,Pr^{1/3}}\right)m_{v,i}c_{p,v}\right]} \quad (23)$$

$$C_f = \frac{\frac{2m_{v,i}}{\rho(u_m-u_i)}}{1-\exp\left[-I(\infty)\left(\frac{1}{Ky^+_{s,0}}\right)^{1/3}\left(\frac{y_s}{\mu}\right)m_{v,i}\right]}. \quad (24)$$

These expressions can be put in a form similar to the classical film theory results by first writing equations (22)–(24) for the limiting case of $m_{v,i} \to 0$ (thus $R_D \to 0$ also). The transfer coefficients $h_{D,0}$, $h_0$ and $C_{f,0}$ then reduce to

$$h_{D,0} = \frac{1}{I(\infty)}\left[\frac{Ky^+_{s,0}}{Sc_t}\right]^{1/3}\left[\frac{\mathscr{D}\,Sc^{1/3}}{y_{s,0}}\right] \quad (25)$$

$$h_0 = \frac{1}{I(\infty)}\left[\frac{Ky^+_{s,0}}{Pr_t}\right]\left[\frac{\lambda\,Pr^{1/3}}{y_{s,0}}\right] \quad (26)$$

$$C_{f,0} = \frac{1}{I(\infty)}[Ky^+_{s,0}]\left[\frac{2\nu}{(u_m-u_i)y_{s,0}}\right]. \quad (27)$$

These coefficients are related by

$$\frac{h_{D,0}}{u_m}Sc^{2/3}\,Sc_t^{1/3} = \frac{h_0}{\rho c_p u_m}Pr^{2/3}\,Pr_t^{1/3} = \frac{C_{f,0}}{2} \quad (28)$$

where we have made the assumption $u_i \ll u_m$. Equation (28) reduces to the Colburn analogy since $Sc_t$ and $Pr_t$ are nearly unity for gases in wall shear flow [13, 17].

In terms of $h_{D,0}$, $h_0$ and $C_{f,0}$, equations (22)–(24) are expressed in the final form

$$\frac{h_D}{h_{D,0}} = \left(\frac{y_{s,0}}{y_s}\right)\frac{\ln(1-R_D)^{-1}}{R_D} \quad (29)$$

$$\frac{h}{h_0} = \frac{\Phi_T}{1-\exp\left(-\Phi_T\frac{y_s}{y_{s,0}}\right)} \quad (30)$$

$$\frac{C_f}{C_{f,0}} = \frac{\Phi}{1-\exp\left(-\Phi\frac{y_s}{y_{s,0}}\right)} \quad (31)$$

with

$$\Phi_T = \frac{m_{v,i}c_{p,v}}{h_0} \quad (32a)$$

$$\Phi = \frac{2m_{v,i}}{\rho u_m C_{f,0}}. \quad (32b)$$

The ratio $y_{s,0}/y_s$ is determined from equation (14). Since this equation is not in a convenient form for condenser design, we combine it with equations (31), (29), (28) and (4) to get

$$\gamma = \frac{y_{s,0}}{y} = \frac{\Psi\exp(-\beta\Psi)}{1-\exp(-\Psi)} \quad (33)$$

where

$$\beta = y^+_{s,0}\sqrt{(St_0\,Pr^{2/3})} \quad (34)$$

$$\Psi = \Phi\frac{y_s}{y_{s,0}} = \frac{c_e/\ell_s}{\rho}Sc^{-2/3}\ln(1-R_D)^{-1}. \quad (35)$$

Equations (29)–(35) are the proposed model for the transfer coefficients. They reduce to the classical film theory correction factors [10] when the parameter $\gamma$ (equation (33)) is taken to be unity. Indeed, this corresponds to the assumption of invariance of film thickness in the derivation of the classical film results. For the present model, however, $\gamma \to 1$ only when $R_D \to 0$; that is, for low mass transfer rates. Otherwise $\gamma$ is always less than unity, and decreases as $R_D$ increases. The growth of the laminar sublayer thickness during mass transfer towards an interface for turbulent flow is a typical result in turbulence theory [12–17]. Here it is made clear by equation (33).

In the 'condensation curve' method [8, 9], the liquid and gas phases are assumed to be approximately in equilibrium, so that [1]

$$R_D \cong R_D^* = \frac{1}{(1-Y_{v,m})P}\left[\frac{dP_v}{dT_m}\right]_{sat}(T_m - T_i). \quad (36)$$

Since the driving force above tends to zero at equilibrium (low mass transfer rates) this method is equivalent to setting the correction factors to unity in equations (29)–(31), and the mass transfer coefficient is shown to be given by [11]

$$h_D^* = \frac{h_0}{\rho c_p} \quad (37)$$

which is equivalent to setting the gas phase Lewis number to unity in the Colburn analogy.

The three models above were applied to predict the global performances for condensation of a steam–air mixture inside a horizontal tube. The procedure adopted was to evaluate the local transfer coefficients from the local conditions of the mixture, and to determine the fluxes from equations (4)–(6) to be used in the integration of suitable mass, enthalpy and momentum balances over a small axial step width. The new conditions obtained from these were used to evaluate the local transfer coefficients in the next step, and so on. Total heat transfer (sensible plus latent) to the

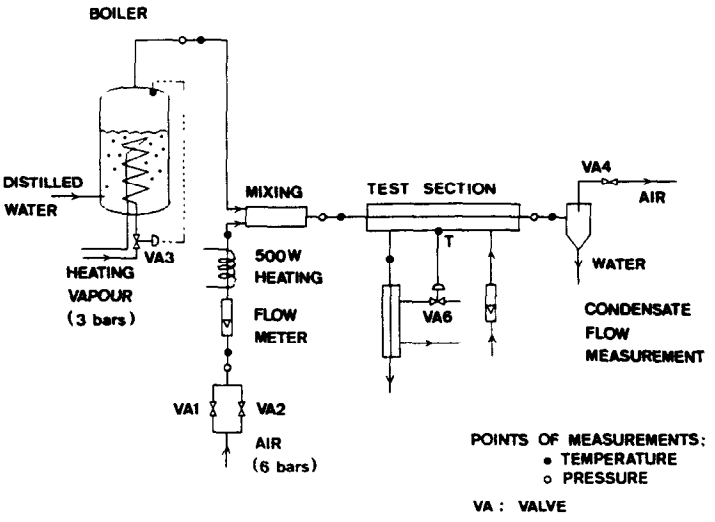


FIG. 2. Plant equipment simplified flow diagram.

coolant was computed in each step, allowing for the evaluation of the heat power at the end of the tube as well as the outlet conditions. Determination of the transfer coefficients generally involved an iterative procedure to evaluate the interface temperature $T_i$ at each step, from which $Y_{v,i}$ is determined (saturated condition at interface). The same method proposed in ref. [4], based on guessing $T_i$, was adopted for the three models. In the case of the proposed model, we first determined $\gamma$ and $\Psi$ (equations (33) and (35)) from the assumed value of $T_i$ before evaluating the correction factors by equations (29)–(31). The entire numerical procedure using a fourth-order Runge–Kutta algorithm and a Newton–Raphson technique to determine $T_i$ is described in detail in ref. [11].

## 3. EXPERIMENTAL APPARATUS AND PROCEDURE

The test section consisted of two horizontal, copper made, smooth concentric tubes of 2 and 3 cm inner diameter. A steam–air mixture flowed in the central tube, with the coolant (water) in the annulus (counter-flow). Two tube lengths were used: 4 m in the first series of runs, and 2 m in the second series.

The entire test facility is shown schematically in Fig. 2. Steam was generated from distilled water in the shell-side of a 2.5 bar shell and tube boiler. Air from a 6 bar control vessel was passed by a flow meter and electrically heated to the same temperature of the saturated steam. Both fluids were passed through a mixing section and the mixture was directed to the test section via a 1 m calming length. At the outlet of the test section, the condensate plus the gas phase were separated in a cyclone, allowing the measurement of the condensate in a calibrated tank beneath the cyclone, whereas the gas phase was in general rejected into the atmosphere.

On the coolant side, distilled water was circulated through a flow meter and directed to the test section. At the outlet, it was cooled in a heat exchanger before returning to the pump. The whole test facility described above was thermally well insulated.

The boiler temperature was automatically regulated to the desired value by the pneumatic valve VA3 acting on the tube side (industrial steam at 3 bar) supply of the boiler. The pressure at the inlet of the test section was also automatically regulated by the pneumatic valve VA4 at the gas phase exit. These two regulations, plus the air flow rate imposed by the flow meter, sufficed to fix the steam flow rate. On the coolant side, the inlet temperature of the water was regulated by the valve VA6, acting on the cold side supply of the heat exchanger. Points of measurement of temperatures and pressures are indicated in Fig. 2. Temperatures were measured by using co-axial chromel–alumel thermocouples previously calibrated ($\pm 0.1$°C). Pressures were measured with a manometer (0.5% accuracy), and the ambient pressure was determined with a standard mercury barometer.

The steam mass flow rate at the inlet of the test section was obtained from the measured condensate and air mass flow rates with the saturation condition of steam at the outlet. Since temperature and pressure at the outlet were known, this method allowed us to evaluate first the steam mass flow rate at the outlet, which was added to the condensate flow rate to obtain the inlet steam mass flow rate. In preliminary tests, as well as in all pure steam runs, arrangements were incorporated to obtain another measure of the inlet steam flow rate by collecting distilled water in the boiler over a measured time interval. The latter method gave results about 5% greater than the former, the difference being mainly attributed to the liquid flow rate rejected in the purge cork before the test section.

The average heat transfer rate (latent plus sensible) to the coolant was obtained from the measured temperature and flow rates via a global enthalpy balance for the mixture. This gives the heat transfer rate to the coolant as

$$Q = M_{\text{cond}}\mathscr{L}_s + (M_{v,\text{in}}c_{p,v} + M_g c_{p,g})(T_{m,\text{in}} - T_{m,\text{out}}) \quad (38)$$

where $M_{\text{cond}}$, $M_{v,\text{in}}$ and $M_g$ are the mass flow rates of, respectively, the condensate, the inlet steam and the noncondensable gas. $\mathscr{L}_s$ is the latent heat.

By dividing $Q$ by the inner surface area of the central tube, we obtained the average heat flux. This method was preferred in relation to the derivation based on the enthalpy balance for the coolant for two reasons: (a) the latent heat contribution (first term in equation (38)) was much greater than the sensible one and (b) the heat loss from the coolant to ambient, although small, was difficult to evaluate precisely.

Some preliminary runs were made in order to verify the validity of the following correlations used in the computer program: (a) Colburn's formula for the Nusselt number for the coolant in the annulus and (b) Nusselt's analysis for uniform wall heat flux condensation of pure steam in the central tube. To verify Colburn's formula, runs were performed with hot water in the central tube, the wall thermal resistance being well known. Results were in very good agreement with calculations using Colburn's correlation on both sides. For condensation of pure steam, we adopted the classical Nusselt analysis with the assumption of uniform wall heat flux. This gives a correlation for the condensate resistance 6% greater than the classical formula for uniform wall temperature. Experimental results obtained [11] for this case showed that the agreement in terms of the calculated and measured mean heat flux was also very good (1–3%). The condensate resistance was low in comparison to that of the coolant (calculated from Colburn's formula).

## 4. RESULTS AND DISCUSSION

### 4.1. *Experiments with a* 4 m *long tube*

Experiments were carried out for inlet air mass fractions varying from 0 to 24%. Average heat flux, outlet temperatures and vapor fractions were measured and compared to the values calculated from the three previously described theories.

For example, Fig. 3 presents the variation of the local heat fluxes calculated from the theories for an input noncondensable gas fraction of 8%, as a function of the condenser length. Also, the measured and computed values of the average heat flux are presented. Although the variation of the local heat flux is different from one theory to the other, the theoretical average values are in agreement with each other and with the experimental data. Such behaviour

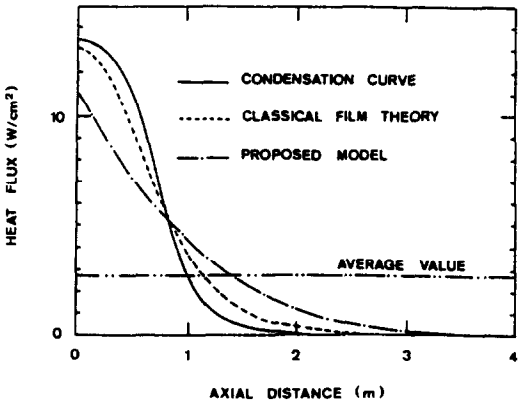


FIG. 3. Heat flux calculated from the three theories (condensation curve, classical film theory and proposed model) as a function of axial distance (4 m long test section). The average values of the three models are identical and represented by the horizontal line.

can also be observed in Fig. 4 where the evolutions of the temperatures are shown.

This can be explained by considering Fig. 5, in which the variations of the condensed mass fractions are presented as a function of the condenser length. It can be seen that in the three cases the vapour is completely condensed at the tube end. Therefore, the average heat fluxes are the same.

Important observations can be made from these curves for condenser dimensioning:

(i) with respect to condensation curve theory, only the first half of the tube is efficient;

(ii) in classical film theory more condenser length is needed;

(iii) in the proposed model, the whole length (4 m) is necessary for a complete condensation.

### 4.2. *Experiments with a* 2 m *long tube*

One way to observe the differences between the three theories is to reduce the tube length. Indeed, in this case, the vapour will not necessarily be completely

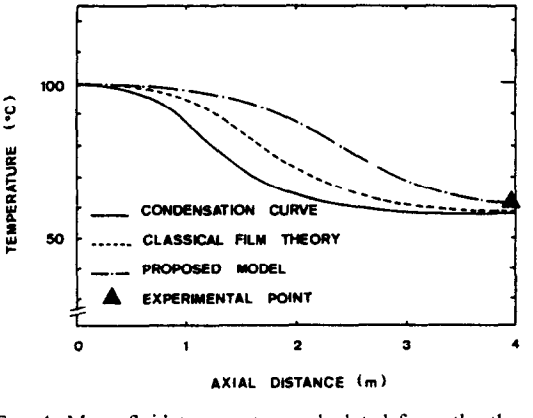


FIG. 4 Mean fluid temperature calculated from the three theories (condensation curve, classical film theory and proposed model) as a function of axial distance (4 m long test section). Comparison with the outlet measured value (▲).

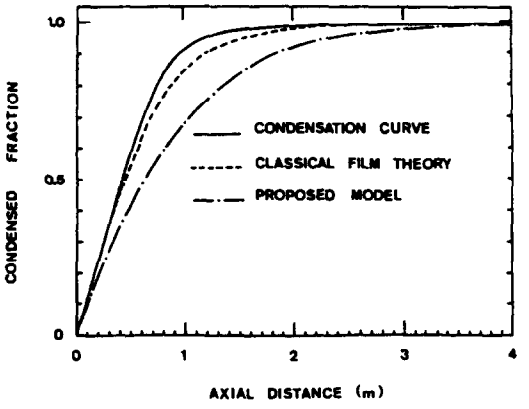


FIG. 5. Condensed fraction calculated from the three theories (condensation curve, classical film theory and proposed model) as a function of axial distance (4 m long test section).

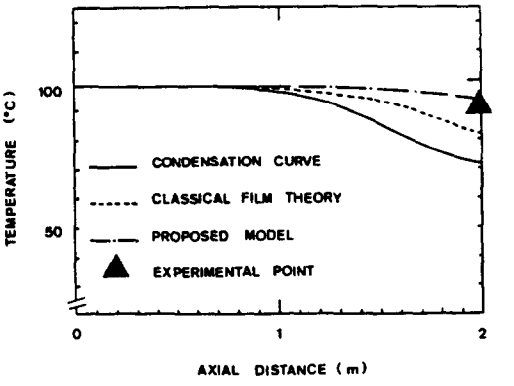


FIG. 7. Mean fluid temperature calculated from the three theories (condensation curve, classical film theory and proposed model) as a function of axial distance (2 m long test section). Comparison with the outlet measured value (▲).

condensed. As the outlet vapour quality is measured, there will be a direct comparison between theoretical and experimental values. Moreover, the evolutions of the local heat flux differ from one theory to the other, so the calculated average heat flux will also be different and will be compared to the experimental values.

Experiments were carried out for inlet air fractions varying from 0 to 9%. The same measurements as for the 4 m long tube were taken. The case of the 5% air fraction is presented in Figs. 6–8. From the results of Fig. 6, the average heat fluxes are calculated and presented in Table 1 together with the proposed model. In Fig. 7, the evolution of the temperatures along the condenser is shown. The outlet temperature is clearly better represented by the proposed model of the variable thickness film. The most decisive test is to compare the outlet vapour qualities as shown in Fig. 8. It is seen that only the proposed model is in close agreement with the experimental value.

This experiment corresponds to an average heat flux of 7.7 W cm$^{-2}$. Other similar experiments were carried out for a different average flux and the results are presented in Fig. 9. The measured outlet mass fraction is reported as a function of the average heat flux together with the theoretical curves calculated from the three theories (condensation curve, classical film theory, proposed model). It can be seen that the best agreement is obtained with the proposed model.

From a general point of view, the previous figures show a progressive improvement from the condensation curve model to the present one. It has already been observed that the differences between the proposed and the other models are greater for the largest values of $R_D$, the three models becoming identical as $R_D \to 0$. In the present analysis, the value of $R_D$ was between 0.5 and 0.9 (Fig. 10), therefore the observed results are different from the theory, as expected. The models were also compared for a lower value of $R_D$, namely $R_D = 0.18$ [11]. In this case, the three models gave close results.

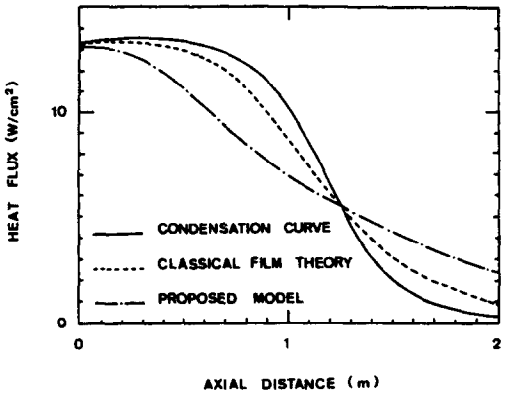


FIG. 6. Heat flux calculated from the three theories (condensation curve, classical film theory and proposed model) as a function of axial distance (2 m long test section).

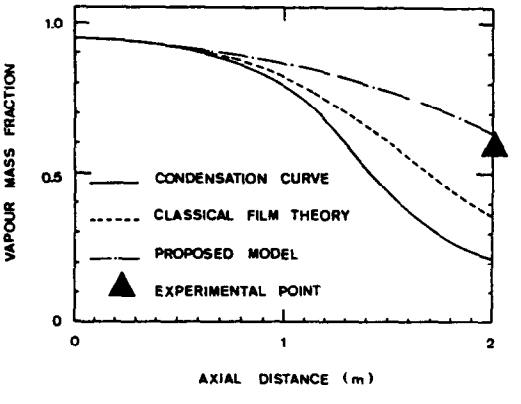


FIG. 8. Vapour quality calculated from the three theories (condensation curve, classical film theory and proposed model) as a function of axial distance (2 m long test section). Comparison with the outlet measured value (▲).

Table 1. Comparison of measured average heat flux with theoretical values calculated from three theories: the condensation curve theory, the classical film theory and the proposed model

| Theory | Average heat flux (W cm$^{-2}$) |
|---|---|
| Condensation curve | 8.21 |
| Classical film theory | 8.09 |
| Proposed model | 7.69 |
| Experimental value | $7.70 \pm 0.06$ |

## 5. CONCLUSION

Analytical models of condensation of a vapour with a noncondensable gas, in turbulent forced convection, can be classified into two categories: (i) the condensation curve methods based on the determination of an equilibrium curve of mixture specific enthalpy as a function of temperature. These methods do not take into account the mass transfer aspect of the problem; (ii) the models based on gaseous film theory, in which are studied mass, heat and momentum transfer in a thin film, enriched with noncondensable gas located near the condensate.

The present model belongs to the second category, whose models are more general and are not based on an equilibrium hypothesis. The classical theories of the gaseous film, as already published, allow one to write the local mass and heat transfer coefficients $h$ and $h_D$ as

$$h_D = h_{D,0} f(R_D)$$
$$h = h_0 g(m_{v,i})$$
$$C_f = C_{f,0} k(m_{v,i})$$

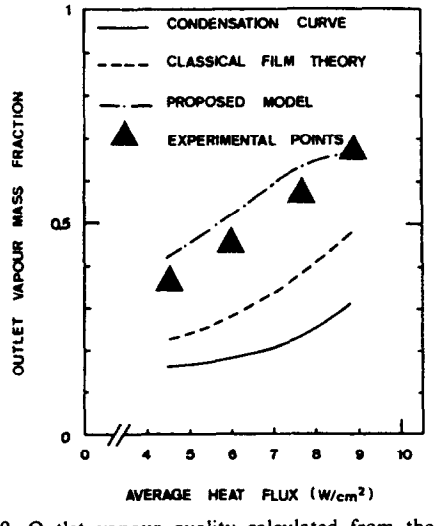


FIG. 9. Outlet vapour quality calculated from the three theories (condensation curve, classical film theory and proposed model) as a function of average heat flux. Comparison with experimental values (▲).

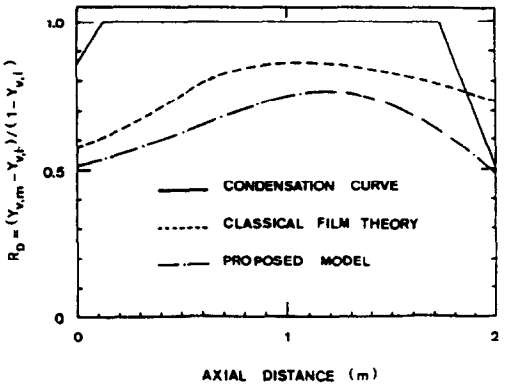


FIG. 10. Mass transfer driving force $R_D$ calculated from the three theories (condensation curve, classical film theory and proposed model) as a function of axial distance (2 m long test section).

where $m_{v,i}$ is the local mass transfer rate. $R_D$ can represent the driving force of the mass transfer and is defined by

$$R_D = \frac{Y_{v,m} - Y_{v,i}}{1 - Y_{v,i}}$$

with

$$0 \leqslant R_D \leqslant Y_{v,m} \leqslant 1.$$

However, such models show some deficiencies due to the hypothesis of a laminar film whose thickness is constant.

The model presented in this work, by taking into account the turbulence near the condensate, allows the description of the variation of the film thickness as a function of the local rate of mass transfer. New analytical formulas (equations (29)–(35)) of the following form have been obtained:

$$h_D = h_{D,0} \gamma f(R_D)$$
$$h = h_0 g'(\gamma, m_{v,i})$$
$$C_f = C_{f,0} k'(\gamma, m_{v,i})$$

where $\gamma$ is the ratio of the film thickness with and without turbulence, which is a function of $R_D$ only.

The two models give the same results as $m_{v,i}$ tends to zero (or $R_D \to 0$). Moreover, when this condition is fulfilled and if the Lewis number equals unity, the condensation curve results are also obtained. The driving force of the mass transfer $R_D$ is an important parameter in calculating the heat and mass transfer coefficients and, thus, in dimensioning condensers.

An experiment has been carried out to test the model, studying the condensation of water vapour in the presence of air inside a horizontal tube. Experimental data have been compared with the three theories (condensation curve, constant thickness and variable film thickness models). The best agreement has been obtained with the proposed model, especially in the case of a high mass transfer rate ($R_D \simeq 0.9$).

From a theoretical point of view, the proposed model gives close agreement with experimental data by taking into account a phenomenon usually neglected in analytical models: the variation of the gaseous film thickness due to turbulence.

From a practical point of view, this new model will permit more accurate dimensioning of condensers.

## REFERENCES


1. J. M. McNaught, An assessment of design methods for condensation of vapors from a non-condensing gas. In *Heat Exchangers: Theory and Practice* (Edited by J. Taborek, G. F. Hewitt and N. Afgan), pp. 35–53. Hemisphere, Washington, DC (1983).
2. D. Butterworth, Condensation of vapor mixtures. In *Heat Exchanger Design Handbook* (Coordinated by D. B. Spalding), Sec. 2.6.3. Hemisphere, Washington, DC (1983).
3. J. G. Collier, Multicomponent boiling and condensation. In *Two-phase Flow and Heat Transfer in the Power and Process Industries* (Edited by A. E. Bergles *et al.*), Chap. 18. Hemisphere, Washington, DC (1981).
4. A. P. Colburn and O. A. Hougen, Design of cooler condensers for mixtures of vapors with non-condensing gases, *Ind. Engng Chem.* **26**, 1178–1182 (1934).
5. A. P. Colburn and T. B. Drew, The condensation of mixed vapors, *Trans. A.I.Ch.E.* **33**, 197–215 (1937).
6. G. Ackermann, Simultaneous heat and mass transfer with transfer with large temperature and partial pressure differences, *VDI ForschHft* **8** (382), 1–116 (1937).
7. R. Krishna, C. B. Panchal, D. R. Webb and I. Coward, An Ackermann–Colburn and Drew type analysis for condensation of multicomponent mixtures, *Lett. Heat Mass Transfer* **3**, 163–172 (1976).
8. L. Silver, Gas cooling with aqueous condensation, *Trans. Inst. Chem. Engrs* **25**, 30–42 (1947).
9. K. J. Bell and M. A. Ghaly, An approximate generalized design method for multicomponent/partial condensers, *A.I.Ch.E. Symp. Ser.* **69** (131), 72–79 (1973).
10. R. B. Bird, W. E. Stewart and E. N. Lightfoot, *Transport Phenomena*, Chap. 21. New York (1960).
11. A. C. Bannwart, Etude théorique et expérimentale de la condensation d'une vapeur en présence d'incondensables, Thèse de Doctorat, Institut National Polytechnique de Grenoble (1988).
12. R. M. Kendall, M. W. Rubesin, T. J. Dahm and M. R. Mendenhall, Mass, momentum and heat transfer within a turbulent boundary layer with foreign gas mass transfer at the surface (Part I), Final Report No. 111, Office of Naval Research, Washington, DC (1964).
13. B. E. Launder and D. B. Spalding, *Mathematical Models of Turbulence*, p. 41. Academic Press, New York (1972).
14. S. V. Patankar and D. B. Spalding, *Heat and Mass Transfer in Boundary Layers* (2nd Edn). Intertext, London (1970).
15. W. M. Kays and R. J. Moffat, The behavior of transpired turbulent boundary layers. In *Studies in Convection—Theory, Measurement and Applications* (Edited by B. E. Launder), Vol. 1. Academic Press, New York (1975).
16. W. P. Jones and U. Renz, Condensation from a turbulent stream onto a vertical surface, *Int. J. Heat Mass Transfer* **17**, 1019–1028 (1974).
17. A. J. Reynolds, *Turbulent Flows in Engineering*, Chaps 3–5. Wiley, New York (1974).
18. F. H. Clauser, The turbulent boundary layer, *Adv. Appl. Mech.* **IV**, 1–51 (1956).


## CONDENSATION D'UNE VAPEUR EN PRESENCE D'INCONDENSABLES: NOUVEAU MODELE DE FILM GAZEUX D'EPAISSEUR VARIABLE


**Résumé**—On présente un modèle de film gazeux permettant le calcul du coefficient de frottement et des coefficients de transfert de chaleur et de masse lors de la condensation d'une vapeur en présence d'un gaz incondensable. Ce modèle tient compte de l'influence de l'intensité du transfert de masse sur l'épaisseur du film gazeux en écoulement turbulent. Les prévisions de ce modèle ainsi que celles de la théorie classique du film et de la méthode de la courbe de condensation sont comparées aux résultats expérimentaux obténus à l'aide d'un mélange saturé vapeur d'eau–air circulant à l'intérieur d'un tube de 2 cm de diamètre dans les conditions suivantes: pression, 1–1,5 bar; fraction massique d'air, 2–30%; vitesse d'entrée, 5–50 m $s^{-1}$. Les résultats montrent que pour de faibles valeurs de la densité de flux (et du taux de condensation) les trois méthodes citées sont en excellent accord avec les données expérimentales. Pour les fortes valeurs de la densité de flux, le modèle proposé rend seul compte correctement des résultats expérimentaux.


## KONDENSATION EINES DAMPFES MIT INERTGASEN—EIN VERBESSERTES FILMMODELL FÜR DIE GASPHASE UNTER BERÜCKSICHTIGUNG DES EINFLUSSES DURCH STOFFTRANSPORT AUF DIE FILMDICKE


**Zusammenfassung**—Es wird ein verbessertes Filmmodell zur Berechnung lokaler Reibungsbeiwerte, Wärme- und Stoffübergangskoeffizienten zur Auslegung von Kondensatoren vorgestellt. Das Modell berücksichtigt den Einfluß des lokalen Stofftransports auf die Grenzschichtdicke einer turbulenten Strömung. Die Berechnungen mit dem vorgestellten Modell sowie nach der klassischen Filmtheorie und der Methode der Kondensationskurve werden mit experimentellen Daten verglichen. Der Vergleich erfolgt für die Kondensation eines gesättigten Wasserdampf/Luft-Gemisches in einem Rohr mit 2 cm Durchmesser und folgenden Randbedingungen: Druck, 1–1,5 bar; Massenanteil der Luft, 2–30%; Geschwindigkeit am Eintritt, 5–50 m $s^{-1}$. Die Ergebnisse zeigen, daß für niedrige Wärmestromdichte (und damit kleinen Werten der Kondensationsrate) alle drei Methoden in guter Übereinstimmung mit den Meßwerten sind. Für hohe Werte der Wärmestromdichte liefert das hier vorgestellte Modell im Gegensatz zu den klassischen Methoden ebenfalls eine exzellente Übereinstimmung.

# КОНДЕНСАЦИЯ ПАРА ПРИ НАЛИЧИИ НЕКОНДЕНСИРУЮЩИХСЯ ВЕЩЕСТВ: УСОВЕРШЕНСТВОВАННАЯ МОДЕЛЬ, УЧИТЫВАЮЩАЯ ВЛИЯНИЕ МАССОПЕРЕНОСА НА ТОЛЩИНУ ПЛЕНКИ

**Аннотация**—Описывается усовершенствованная модель, позволяющая рассчитать локальные значения трения в пограничном слое, а также коэффициенты тепло- и массопереноса при конструировании конденсатора. Модель учитывает влияние интенсивности локального массопереноса на толщину пленки при турбулентном течении. Расчеты по предложенной модели, а также с применением классических методов пленочной теории и кривой конденсации сравниваются с экспериментальными данными для течения насыщенной паровоздушной смеси в трубе диаметром 2 см при следующих условиях: давление 1–1,5 бар; весовая доля воздуха 2–30%; скорость на входе 5–50 м $\cdot$ с$^{-1}$. Результаты показывают, что при низких значениях плотности тепловых потоков (а также малых скоростях конденсации) три указанных метода хорошо согласуются с экспериментом. При высоких же значениях плотности тепловых потоков с экспериментом хорошо согласуются результаты, полученные по предложенной модели, а не с применением классических методов.